Available online at www.sciencedirect.com
ScienceDirect
International Journal of Hydrogen Energy 32 (2007) 4966–4972
International Journal of HYDROGEN ENERGY
www.elsevier.com/locate/ijhydene

Cyclic hydrogen absorption–desorption characteristics of TiCrV and $Ti_{0.8}Cr_{1.2}V$ alloys

H.C. Lin[a,*], K.M. Lin[b], K.C. Wu[b], H.H. Hsiung[c], H.K. Tsai[c]

[a]*Department of Materials Science and Engineering, National Taiwan University, Taipei, Taiwan*
[b]*Department of Materials Science and Engineering, Feng Chia University, Taichung, Taiwan*
[c]*Department of Product Development, Taiwan Textile Research Institute, Taipei, Taiwan*

Received 5 July 2007; received in revised form 23 July 2007; accepted 23 July 2007
Available online 10 September 2007

Abstract

The cyclic hydrogen absorption–desorption characteristics of TiCrV and $Ti_{0.8}Cr_{1.2}V$ alloys are investigated. Experimental results show that the cyclic hydrogen capacity increases with increasing hydrogen-desorption temperature for both TiCrV and $Ti_{0.8}Cr_{1.2}V$ alloys. The $Ti_{0.8}Cr_{1.2}V$ and TiCrV alloys can maintain steady cyclic hydrogen capacities of about 2.5 wt% and 2.0 wt%, respectively, even after 15 cycles with hydrogen absorption at 25 °C and hydrogen desorption at 400 °C. The hydrogenation for both TiCrV and $Ti_{0.8}Cr_{1.2}V$ alloys includes the processes of first saturated solid-solution and then forming $TiCr_{1.8}H_{5.3}$ and TiH_2 hydrides. The $TiCr_{1.8}H_{5.3}$ hydride has better reversibility than TiH_2 hydride during the hydrogen absorption–desorption.

Keywords: Hydrogen storage alloy; Ti–Cr–V alloy; Hydride

1. Introduction

Hydrogen is a clean, low polluting, renewable energy source [1–3]. It is considered to be a solution to replace the diminishing fossil fuels and beneficial in the protection of the global environment. From the application point of view, hydrogen storage is one of the keystones to "Hydrogen Economy". There are various methods for storing hydrogen [4], including high-pressure compressed gas, low-temperature liquid hydrogen and solid storage of metal hydrides in hydrogen storage alloys (HSAs). Of these methods, metal hydrides have recently attracted much attention due to their small volume, low equilibrium pressure and high safety.

Ti–Cr–V alloys have recently been investigated as important HSAs [5–14]. These alloys exhibit a BCC solid solution structure and their hydrogen storage capacity is larger than that of intermetallic alloys. Maximum hydrogen absorbing capacity of these alloys can reach about 3.7 wt%. However, their rechargeable hydrogen capacity is limited, especially at lower temperatures of hydrogen desorption. In the past decade, many researchers have strived to improve the hydrogen storage characteristics of these Ti–Cr–V alloys. It has been understood that the hydrogen storage properties of these Ti–Cr–V alloys are significantly influenced by the melting methods and thermal history [15–17], heat-treating condition [18], chemical compositions and additional elements [19–24]. In the present study, the TiCrV and $Ti_{0.8}Cr_{1.2}V$ HSAs are selected, because of their optimal representation of these Ti–Cr–V alloys. The cyclic hydrogen absorption–desorption characteristics of TiCrV and $Ti_{0.8}Cr_{1.2}V$ alloys are systematically investigated. The crystal structures of hydrogenated and dehydrogenated TiCrV and $Ti_{0.8}Cr_{1.2}V$ alloys with different amount of hydrogen absorption and with cyclic hydrogen absorption–desorption will also be studied.

2. Experimental procedure

The TiCrV and $Ti_{0.8}Cr_{1.2}V$ HSAs were prepared by vacuum melting. The as-cast alloys were analyzed using inductively coupled plasma atomic emission spectroscopy (ICP-AES). Their chemical compositions, being presented in Table 1, were

* Corresponding author. Tel.: +886 2 3366 4532; fax: +886 2 2363 4562.
E-mail address: hclinntu@ntu.edu.tw (H.C. Lin).

0360-3199/$ - see front matter © 2007 International Association for Hydrogen Energy. Published by Elsevier Ltd. All rights reserved.
doi:10.1016/j.ijhydene.2007.07.057

Table 1
ICP-AES measured chemical compositions of TiCrV and $Ti_{0.8}Cr_{1.2}V$ alloys

Alloy	Element (at%)		
	Ti	Cr	V
TiCrV	32.76	33.75	33.49
$Ti_{0.8}Cr_{1.2}V$	28.01	39.47	32.52

found to be virtually the same as the nominal ones. The as-cast alloys were crushed below a 150 mesh and then their crystal structures were identified by utilizing the Philips PW1710 X-ray diffractometer under the conditions of Cu Kα radiation, 40 kV tube voltage and 30 mA current. The surface morphologies of the alloy particles were inspected by field emission gun scanning electron microscopy (FEG-SEM). The characteristics of hydrogen storage were analyzed using a computer-controlled automatic "PCI Monitoring System" (GFE, Germany) with an accuracy of 1%. During their preparation, the TiCrV and $Ti_{0.8}Cr_{1.2}V$ particles will readily form the surface passivation layers [25], including the metal–oxide, hydride and surface contaminants of CO, H_2O, etc. Thus, an activation process is necessary for TiCrV and $Ti_{0.8}Cr_{1.2}V$ alloys to efficiently absorb hydrogen gas. The activation treatments were as follows [23]. The alloy particles were individually put into testing vessels and evacuated at 400 °C for 2 h. High purity hydrogen gas was introduced into the vessels up to a pressure of 5 MPa at 25 °C and then evacuated at 400 °C. After the activation treatments, these alloy particles were executed by the experiments of cyclic hydrogen absorption–desorption. Each cycle of hydrogen absorption–desorption is carried out as follows. They were purged into hydrogen gas with 5 MPa pressure at 25 °C for 30 min, and then dehydrogenated by vacuum pumping at a set temperature (25–400 °C) for 1 h.

3. Results and discussion

3.1. Cyclic hydrogen absorption–desorption characteristics of TiCrV and $Ti_{0.8}Cr_{1.2}V$ alloys

Fig. 1(a) and (b) shows the cyclic hydrogen capacities for the TiCrV and $Ti_{0.8}Cr_{1.2}V$ alloys, respectively, which are subjected to cyclic hydrogen–absorption at 25 °C and hydrogen desorption at various temperatures. As shown in Fig. 1(a) and (b), the saturated capacities of first hydrogen absorption at 25 °C can reach 3.54 and 3.20 wt% for TiCrV and $Ti_{0.8}Cr_{1.2}V$ alloys, respectively. However, these values are significantly reduced to be 0.98 and 2.02 wt%, respectively, in the second hydrogen absorption. These phenomena can be explained as below. It is known that Ti atom has a bigger radius than the Cr atom ($R_{Ti} = 2.00$ Å, $R_{Cr} = 1.85$ Å). The TiCrV alloy has more Ti atoms and less Cr atoms than the $Ti_{0.8}Cr_{1.2}V$ alloy. This will make TiCrV alloy have a bigger lattice constant, i.e., a wider spacing of crystal planes. Hence, TiCrV alloy is able to absorb more H atoms to form the metal hydride during the first hydrogenation process, and its saturated capacity of first hydrogen absorption is higher than that of $Ti_{0.8}Cr_{1.2}V$ alloy.

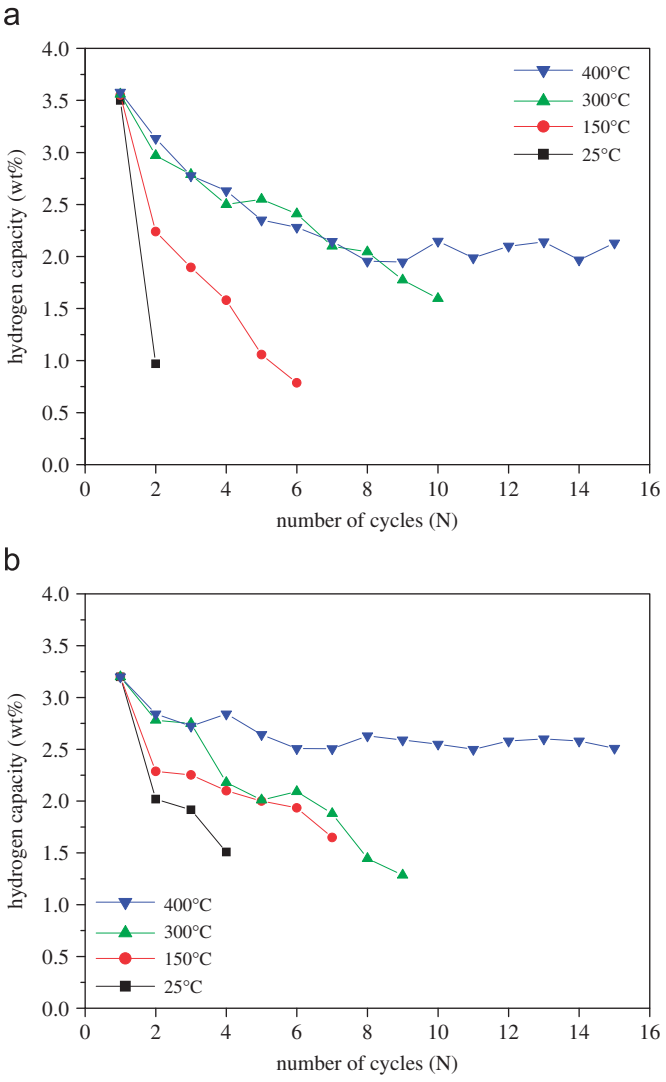

Fig. 1. The cyclic hydrogen capacities for the (a) TiCrV and (b) $Ti_{0.8}Cr_{1.2}V$ alloys. These alloys are subjected to cyclic hydrogen absorption at 25 °C and hydrogen desorption at various temperatures.

However, the Ti–H bonding is stronger than Cr–H bonding in their hydrogenated state at 25 °C. Meanwhile, more Ti–H bonding will occur for TiCrV alloy due to its higher Ti/Cr ratio. These features demonstrate that less quantity of H atoms within the TiCrV alloy can release out during the dehydrogenation process at 25 °C. Hence, the saturated capacity of the second hydrogen absorption of TiCrV is lower than $Ti_{0.8}Cr_{1.2}V$ alloy.

In Fig. 1(a) and (b), one can also find that the cyclic hydrogen capacities for both alloys increase with increasing hydrogen-desorption temperature. Meanwhile, the hydrogen capacities decrease rapidly with increasing hydrogen absorption–desorption cycle if the hydrogen-desorption temperature is lower than 300 °C. However, both alloys can have stable cyclic hydrogen capacities at hydrogen-desorption temperature of 400 °C. When comparing the cyclic hydrogen capacities at 400 °C in Fig. 1(a) and (b), the $Ti_{0.8}Cr_{1.2}V$ alloy exhibits a better performance of cyclic hydrogen absorption–desorption than TiCrV alloy. The $Ti_{0.8}Cr_{1.2}V$ and TiCrV alloys can maintain

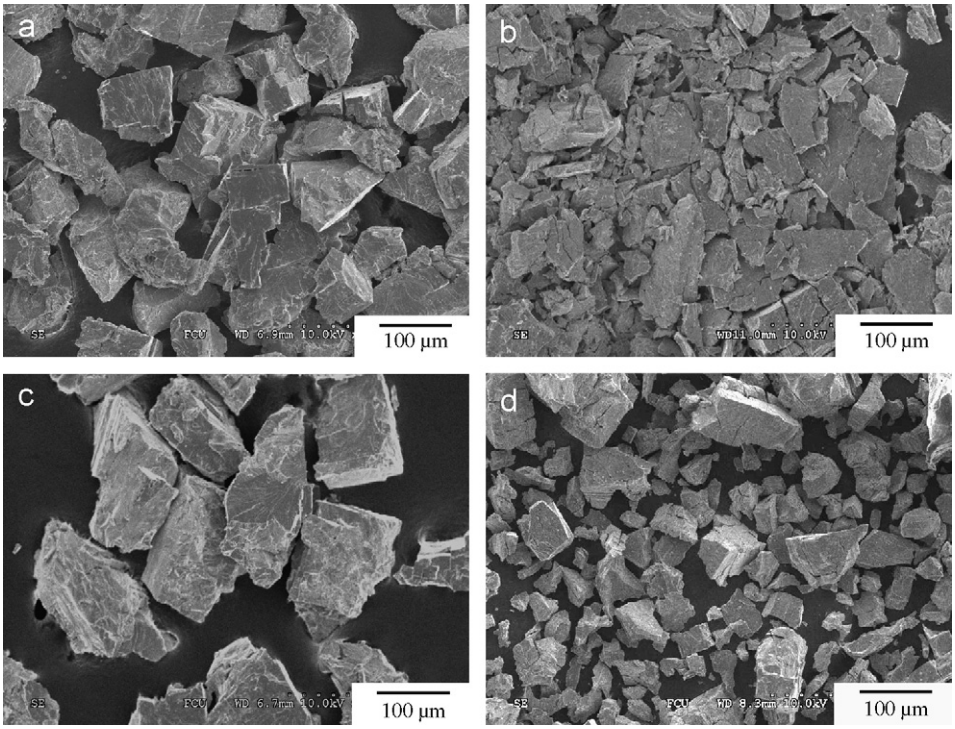

Fig. 2. The SEM surface morphologies of TiCrV and $Ti_{0.8}Cr_{1.2}V$ alloys. (a) TiCrV, as-crushed, (b) TiCrV, after 15 cyclic hydrogen absorption–desorption, (c) $Ti_{0.8}Cr_{1.2}V$, as-crushed and (d) $Ti_{0.8}Cr_{1.2}V$, after 15 cyclic hydrogen absorption–desorption.

steady cyclic hydrogen capacities of about 2.5 and 2.0 wt%, respectively, after 15 cycles with hydrogen absorption at 25 °C and hydrogen desorption at 400 °C.

Fig. 2(a)–(d) shows the SEM surface morphologies of TiCrV and $Ti_{0.8}Cr_{1.2}V$ alloys in the states of as-crushed and after 15 cycles of hydrogen absorption–desorption, respectively. As can be seen in these SEM micrographs, the particle sizes have reduced from 50–150 to 10–120 μm after 15 cycles. The lattice expansion due to the occupation of hydrogen atoms leads to the splitting of the alloy particles into finer ones, referred to as pulverization [26,27]. Carefully examining the SEM surface morphologies in Fig. 2(b) and (d), the pulverized TiCrV and $Ti_{0.8}Cr_{1.2}V$ alloys exhibit different shapes of platelet and polygonal particles, respectively. This phenomenon has not been clearly understood, but these different shapes of pulverized particles of TiCrV and $Ti_{0.8}Cr_{1.2}V$ alloys are considered to have important effects on their cyclic hydrogen capacities.

3.2. *Crystal structures of hydrogenated and dehydrogenated TiCrV and $Ti_{0.8}Cr_{1.2}V$ alloys with different amount of hydrogen absorption*

Prior to discuss the crystal structures of TiCrV and $Ti_{0.8}Cr_{1.2}V$ alloys with cyclic hydrogen absorption–desorption, it is valuable to understand more the crystal structures of these alloys with different amount of hydrogen absorption. Fig. 3(a) and (b) shows the XRD patterns of TiCrV alloy in hydrogenated and dehydrogenated states, respectively, with various amounts of hydrogen absorption at 25 °C. In Fig. 3(a) and (b), it can be seen that both as-crushed TiCrV and $Ti_{0.8}Cr_{1.2}V$ alloys exhibit a crystal structure of single BCC phase. The addition of V into TiCr alloy shall reduce its transformation temperature and inhibit the formation of Laves phases during the casting process [21], and hence both TiCrV and $Ti_{0.8}Cr_{1.2}V$ alloys exhibit a single BCC phase. In Fig. 3(a), the TiCrV alloy with 1.02 wt% hydrogen absorption still exhibits a BCC structure, which is similar to that of as-crushed alloy. Whilst, the corresponding XRD peaks shift to lower 2θ positions for the 1.02 wt% hydrogenated alloy. This indicates that the solid solution of hydrogen atoms will increase the spacing of lattice planes. The lattice constant increases from 3.0568 to 3.1658 Å and leads to a volume expansion $[(a_2^3 - a_1^3)/a_1^3 \times 100\%]$ of 11.09%. When the hydrogen absorption rises up to 1.50 wt%, a little FCC hydride of $TiCr_{1.8}H_{5.3}$ appears in the XRD patterns. With increasing the hydrogen absorption up to 2.02 and 2.49 wt%, more $TiCr_{1.8}H_{5.3}$ hydride and less BCC solid-solution phase are found in the hydrogenated alloy. When the hydrogen absorption reaches a saturated value of 3.55 wt%, the BCC solid-solution phase completely disappears and another BCC hydride of TiH_2 forms, which coexists with the $TiCr_{1.8}H_{5.3}$ hydride. The main XRD peak position of TiH_2 hydride, $2\theta = 39.9°$, is found to nearly overlap with that of the BCC solid-solution phase. As reported in a previous paper [24], the Ti–Cr–V alloy with high V content will prohibit the formation of TiH_2 hydride during the hydrogenation process. This phenomenon can demonstrate why the TiH_2 hydride only appears after the saturated formation of $TiCr_{1.8}H_{5.3}$ hydride, as shown in Fig. 3(a).

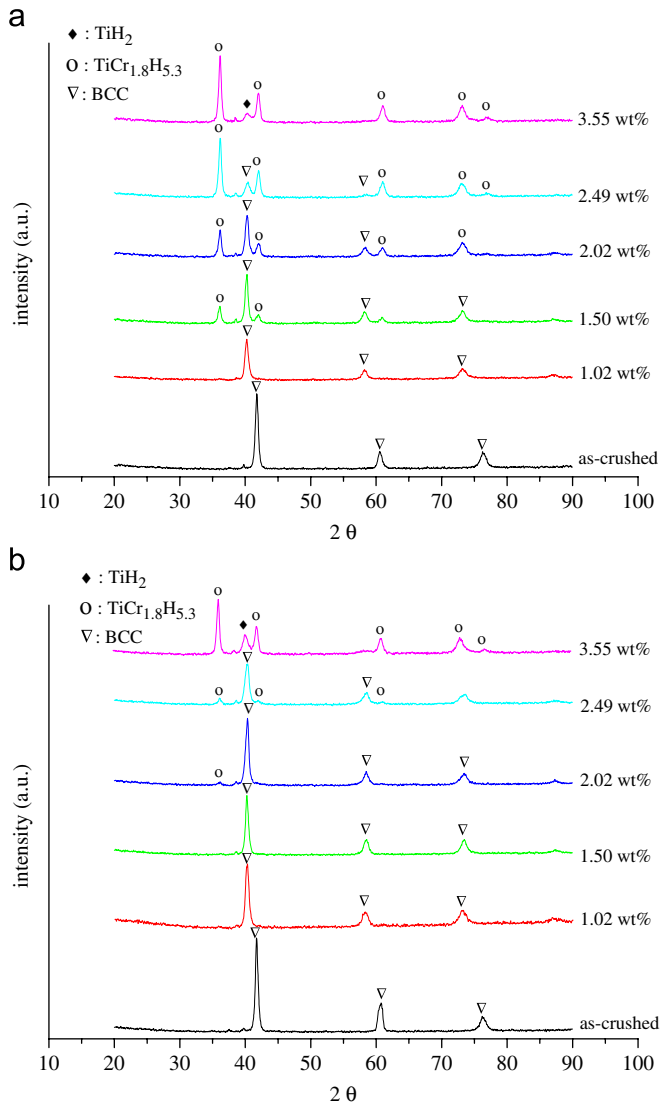

Fig. 3. XRD patterns of TiCrV alloy in (a) hydrogenated and (b) dehydrogenated states, with various amounts of hydrogen absorption at 25 °C.

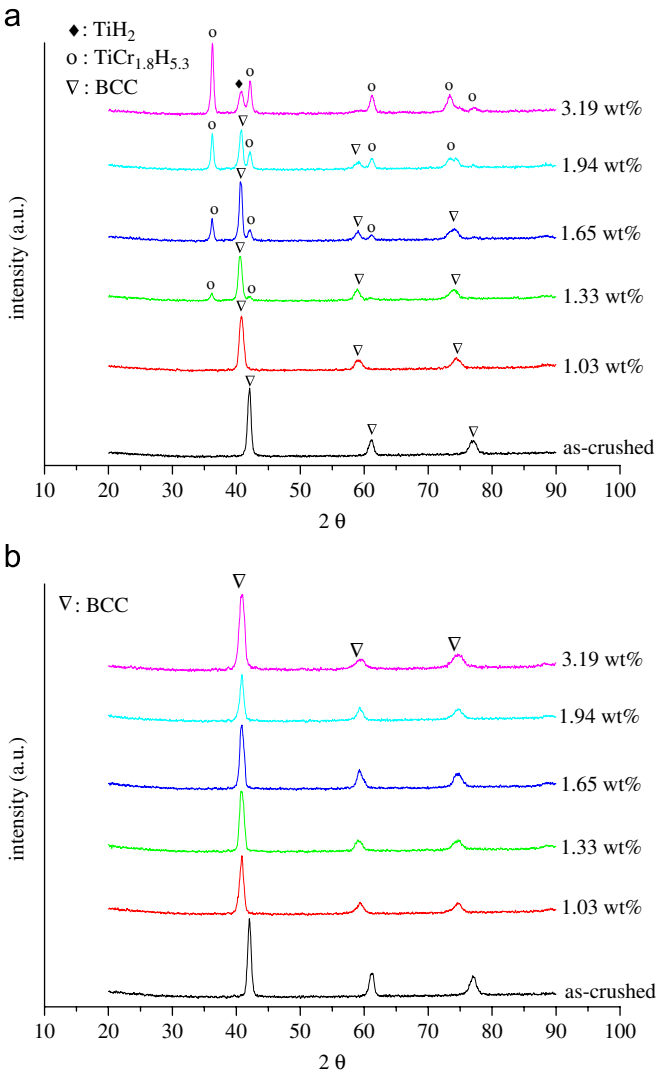

Fig. 4. XRD patterns of $Ti_{0.8}Cr_{1.2}V$ alloy in (a) hydrogenated and (b) dehydrogenated states, with various amounts of hydrogen absorption at 25 °C.

As calculated from the XRD patterns in Fig. 3(b), the lattice constant and volume expansion of the dehydrogenated TiCrV alloy with 1.02 wt% hydrogen absorption are 3.1573 Å and 10.43%, respectively, which are only a little lower than those in the hydrogenated state. It indicates that the dehydrogenation of BCC solid-solution phase is not obvious. For the dehydrogenated TiCrV alloy with 1.50 wt% hydrogen absorption, a BCC solid-solution phase is still observed but the $TiCr_{1.8}H_{5.3}$ hydride has disappeared, as compared to those XRD patterns in Fig. 3(a). It indicates that the $TiCr_{1.8}H_{5.3}$ hydride can exhibit a good reversibility during the hydrogen absorption–desorption. Even the quantity of hydrogen absorption rises up to 2.02 and 2.49 wt%; there is only a little residual $TiCr_{1.8}H_{5.3}$ hydride in the dehydrogenated state. For the TiCrV alloy with saturated hydrogen absorption of 3.55 wt%, a lot of $TiCr_{1.8}H_{5.3}$ and TiH_2 hydrides reside after hydrogen desorption, as shown in Fig. 3(b).

Fig. 4(a) and (b) shows the XRD patterns of $Ti_{0.8}Cr_{1.2}V$ alloy in hydrogenated and dehydrogenated states, respectively, with various amounts of hydrogen absorption at 25 °C. The XRD patterns in Fig. 4(a) have similar results as those shown in Fig. 3(a) for the TiCrV alloy. The increment of lattice constant and volume expansion are also clearly found from the 2θ peak positions in the 1.03 wt% hydrogenated alloy. In addition, the $TiCr_{1.8}H_{5.3}$ hydride forms if the hydrogen absorption is higher than 1.33 wt%, and both TiH_2 and $TiCr_{1.8}H_{5.3}$ hydrides coexist in the 3.19 wt% hydrogenated alloy. In Fig. 4(b) for the dehydrogenated states of $Ti_{0.8}Cr_{1.2}V$ alloy, one can find that all $TiCr_{1.8}H_{5.3}$ hydride disappears even though this alloy has been subjected to a saturated hydrogen absorption of 3.19 wt%. This feature indicates that the reversibility of $TiCr_{1.8}H_{5.3}$ hydride in $Ti_{0.8}Cr_{1.2}V$ alloy is better than in TiCrV alloy.

3.3. Crystal structures of hydrogenated and dehydrogenated TiCrV and $Ti_{0.8}Cr_{1.2}V$ alloys with cyclic hydrogen absorption–desorption

Fig. 5(a) and (b) shows the XRD patterns of TiCrV alloy in hydrogenated and dehydrogenated states, respectively,

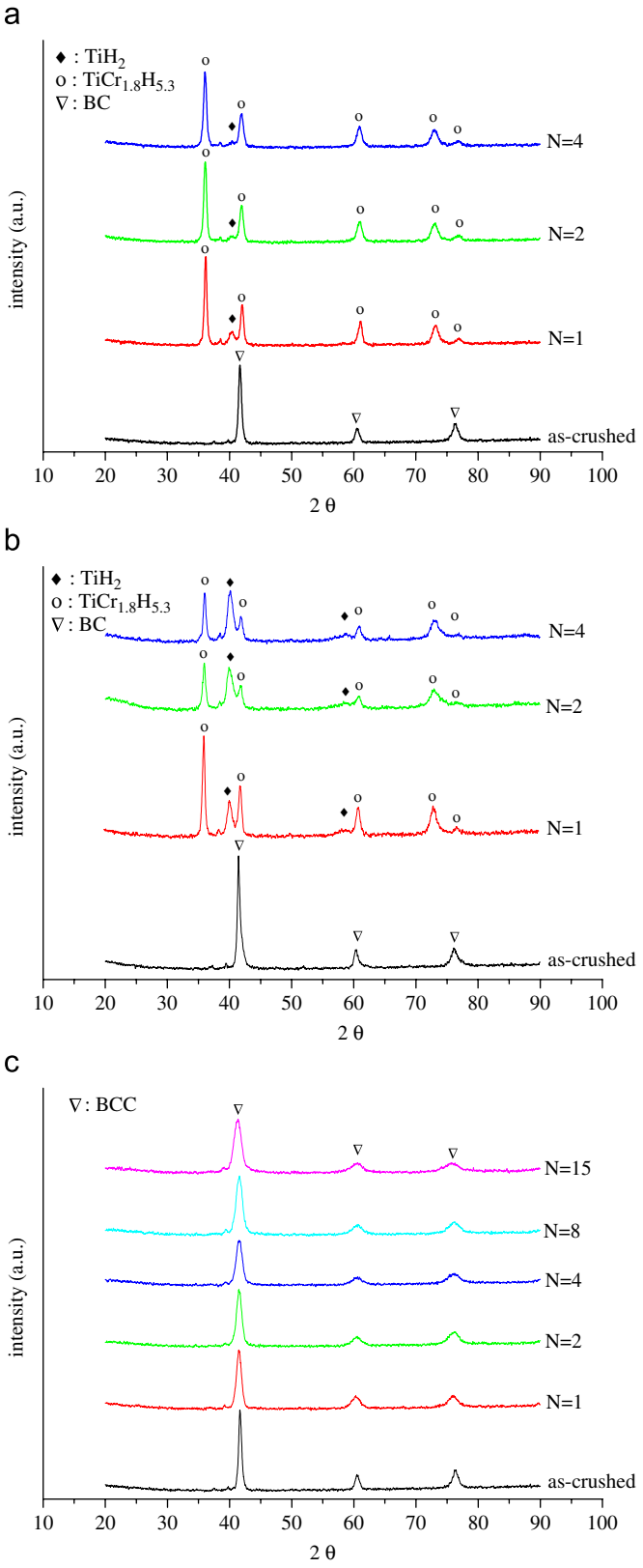

Fig. 5. XRD patterns for the (a) hydrogenated and (b) dehydrogenated TiCrV alloys, which have been subjected to cyclic hydrogen absorption–desorption at 25 °C. (c) XRD patterns for the dehydrogenated TiCrV alloy, which has been subjected to cyclic hydrogen absorption at 25 °C and hydrogen desorption at 400 °C.

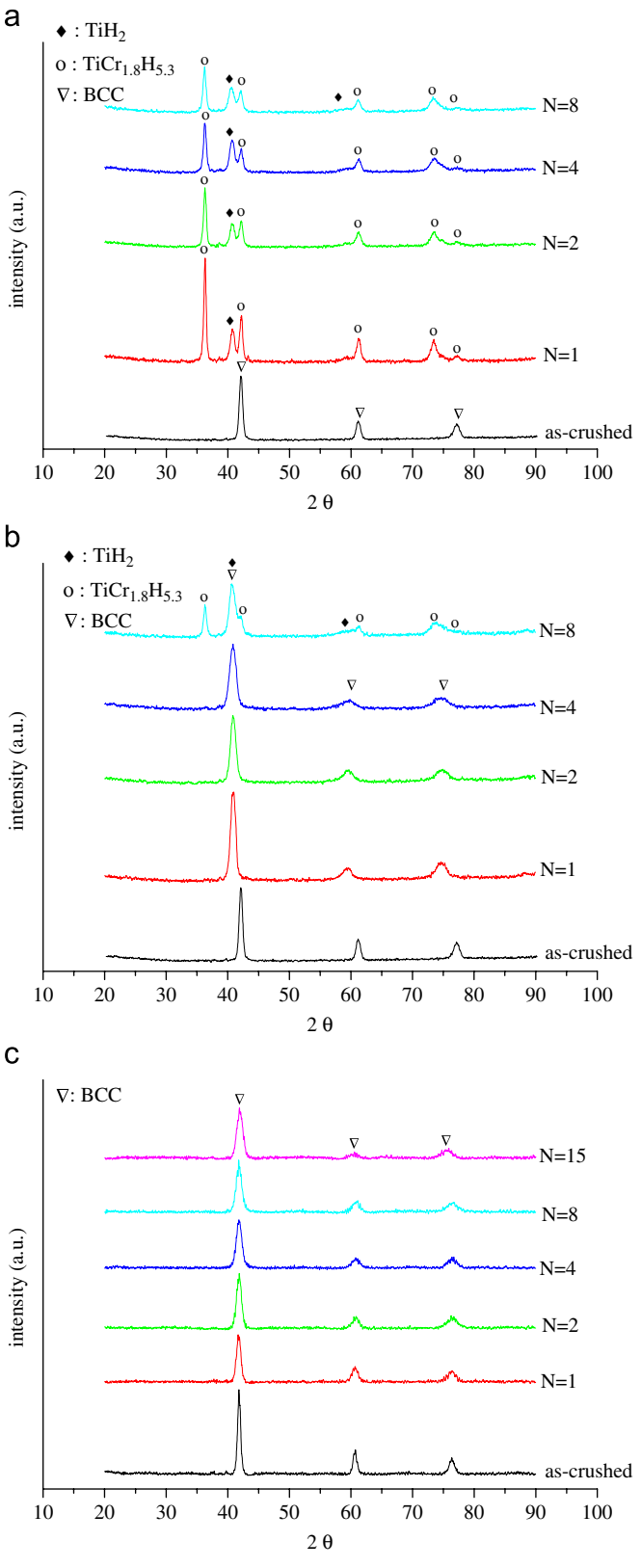

Fig. 6. XRD patterns for the (a) hydrogenated and (b) dehydrogenated $Ti_{0.8}Cr_{1.2}V$ alloys, which have been subjected to cyclic hydrogen absorption–desorption at 25 °C. (c) XRD patterns for the dehydrogenated $Ti_{0.8}Cr_{1.2}V$ alloy, which has been subjected to cyclic hydrogen absorption at 25 °C and hydrogen desorption at 400 °C.

with cyclic saturated hydrogen absorption–desorption at 25 °C. As shown in Fig. 5(a), there is no obvious variation of XRD peak intensities of both $TiCr_{1.8}H_{5.3}$ and TiH_2 hydrides after cyclic saturated hydrogen absorption–desorption at 25 °C. In Fig. 5(b), although the XRD patterns also exhibits the coexistence of $TiCr_{1.8}H_{5.3}$ and TiH_2 hydrides in the dehydrogenated states, the $TiH_2/TiCr_{1.8}H_{5.3}$ ratios are higher than those in the hydrogenated states. It indicates that the $TiCr_{1.8}H_{5.3}$ is easier than TiH_2 to release the hydrogen atoms during the dehydrogenation process. More TiH_2 hydride resides with increasing cycles of saturated hydrogen absorption–desorption, and hence $TiH_2/TiCr_{1.8}H_{5.3}$ ratio also increases with increasing cycles, as shown in Fig. 5(b).

Fig. 5(c) shows the XRD patterns of dehydrogenated TiCrV alloy, which has been subjected to cyclic hydrogen absorption at 25 °C and hydrogen desorption at 400 °C. The XRD patterns in Fig. 5(c) only exhibit the existence of BCC matrix, and their 2θ positions are nearly the same for the as-crushed and dehydrogenated TiCrV specimens even after 15 cycles. This means that the performance of hydrogen desorption at 400 °C is quite excellent. No hydrides reside and even very few irreversible H atoms exist in the BCC matrix.

Fig. 6(a) and (b) shows the XRD patterns of $Ti_{0.8}Cr_{1.2}V$ alloy in hydrogenated and dehydrogenated states, respectively, with cyclic saturated hydrogen absorption–desorption at 25 °C. As shown in Fig. 6(a), the $TiCr_{1.8}H_{5.3}$ and TiH_2 hydrides coexist in the hydrogenated $Ti_{0.8}Cr_{1.2}V$ alloy. With increasing cycles of hydrogen absorption–desorption at 25 °C, the ratio of $TiCr_{1.8}H_{5.3}/TiH_2$ decreases due to the easier dehydrogenation of $TiCr_{1.8}H_{5.3}$ hydride. In Fig. 6(b), the XRD patterns exhibit that only BCC matrix, but no hydrides, exists in the dehydrogenated $Ti_{0.8}Cr_{1.2}V$ alloy even after a few cycles. It indicates that the $Ti_{0.8}Cr_{1.2}V$ alloy can still have fair performance of dehydrogenation from the hydrides at 25 °C. The shift of XRD peaks to lower 2θ positions means that the BCC matrix comprises some H atoms, which exhibits a lattice expansion. After 8 cycles, the XRD peaks of $TiCr_{1.8}H_{5.3}$ and TiH_2 hydrides begin to appear in Fig. 6(b). This feature indicates that the $TiCr_{1.8}H_{5.3}$and TiH_2 hydrides have been accumulated to enough amounts to be detected by XRD analysis.

Fig. 6(c) shows the XRD patterns of dehydrogenated $Ti_{0.8}Cr_{1.2}V$ alloy, which has been subjected to cyclic hydrogen absorption at 25 °C and hydrogen desorption at 400 °C. The XRD patterns in Fig. 6(c) only exhibit the existence of BCC matrix, and their 2θ positions are nearly the same for the as-crushed and dehydrogenated $Ti_{0.8}Cr_{1.2}V$ specimens even after 15 cycles. These phenomena are similar to those shown in Fig. 5(c) for TiCrV alloy. Namely, both TiCrV and $Ti_{0.8}Cr_{1.2}V$ alloys can have excellent performance of hydrogen desorption at 400 °C. These results are consistent with those shown in Fig. 1(a) and (b).

4. Conclusions

1. The cyclic hydrogen capacity increases with increasing hydrogen-desorption temperature for both TiCrV and $Ti_{0.8}Cr_{1.2}V$ alloys. $Ti_{0.8}Cr_{1.2}V$ alloy has a better performance of cyclic hydrogen absorption–desorption than TiCrV alloy. The $Ti_{0.8}Cr_{1.2}V$ and TiCrV alloys can maintain steady cyclic hydrogen capacities of about 2.5 and 2.0 wt%, respectively, after 15 cycles with hydrogen absorption at 25 °C and hydrogen desorption at 400 °C.
2. The hydrogenation for both TiCrV and $Ti_{0.8}Cr_{1.2}V$ alloys includes the processes of first saturated solid-solution and then forming $TiCr_{1.8}H_{5.3}$ and TiH_2 hydrides. The $TiCr_{1.8}H_{5.3}$ hydride has better reversibility than TiH_2 hydride during the hydrogen absorption–desorption. The accumulation of residual hydrides will reduce the alloy's cyclic hydrogen capacity.

Acknowledgment

The authors would like to sincerely acknowledge the financial support of this study by Taiwan Textile Research Institute and Feng Chia University, Taiwan, under the Grant FCU-94GB47.

References

[1] Elam CC, Padro CEG, Sandrock G, Luzzi A, Lindblad P, Hagen EF. Realizing the hydrogen future: the International Energy Agency's efforts to advance hydrogen energy technologies. Int J Hydrogen Energy 2003;28:601–7.
[2] Fujii H, Orimo S. Hydrogen storage properties in nano-structured magnesium- and carbon-related materials. Physica B 2004;328:77.
[3] Schlapbach L, Zuttel A. Hydrogen-storage materials for mobile applications. Nature 2001;414:353.
[4] Zuttel A. Hydrogen storage methods. Naturwissenshaften 2004;91:157–72.
[5] Tominaga Y, Nishimura S, Amemiya T, Fuda T, Tamura T, Kuriiwa T. et al. Protium absorption–desorption properties of Ti–V–Cr–(Mn, Ni) alloys. Mater Trans JIM 2000;41:617.
[6] Cho SW, Han CS, Park CN, Akiba E. Synthesis and emission spectra of $Ba_4In_{1.98}Nd_{0.02}O_7$ and $Ba_4In_{1.98}Er_{0.02}O_7$. J Alloys Compds 1999;388:294.
[7] Tamura T, Kazumi T, Kamegawa A. Protium absorption properties and protide formations of Ti–Cr–V alloys. J Alloys Compds 2003;356–357:505–9.
[8] Tamura T, Kamegawa A, Takamura H, Okada M. Protium absorption–desorption properties of Ti–V–Cr alloys with a BCC structure. Mater Trans 2002;43:410–3.
[9] Cho SW, Enoki H, Kabutomori T, Park CN, Akiba E. Isotope effect on structural transitions of $Ti_{1.0}Mn_{0.9}V_{1.1}H_X(D_X)$ and $Ti_{1.0}Cr_{1.5}V_{1.7}H_X(D_X)$ with hydrogenation. J Alloys Compds 2001;319:196.
[10] Xu YH, Chen CP, Wang XL, Wang QD. The electrode properties of the $Ti_{1.0}Zr_{0.2}Cr_{0.4}Ni_{0.8}V_{0.8-x}Al_x$ ($x=0.0$, 0.2, 0.4 and 0.6) alloys. Mater Chem Phys 2003;77:1–5.
[11] Okada M, Tamura M, Takamura H, Kamegawa A. Ti–V–Cr BCC alloys with high protium content. J Alloys Compds 2002;330–332:511–6.
[12] Peretti HA, Visintin A, Magni LV, Corso HL, Ganboa JA, Serafini D. Hydrogen absorption behavior of multicomponent zirconium based AB_2 alloys with different chromium–vanadium ratio. J Alloys Compds 2003;354:181.
[13] Verbetsky VN, Mitrokhin SV, Movlaev EA. Synthesis and properties of multicomponent hydrides with high density. J Alloys Compds 1999;293–295:421–5.
[14] Mitrokhin SV, Bezuglaya TN, Verbetsky VN. Structure and hydrogen sorption properties of (Ti,Zr)–Mn–V alloys. J Alloys Compds 2002;330–332:146–51.
[15] Itoh H, Arashima H, Kubo K, Kabutomori T. The influence of microstructure on hydrogen absorption properties of Ti–Cr–V alloys. J Alloys Compds 2002;330–332:287.

[16] Kazumi T, Tamura T, Kamegawa A, Takamura H, Okada M. Effects of absorption–desorption cycles on protium absorption properties in Ti–Cr–M alloys (M = V, Mo, Al). Mater Trans 2003;44:1588–92.
[17] Akiba E, Iba H. Hydrogen absorption by Laves phase related BCC solid solution. Intermetallics 1998;6:461–70.
[18] Okada M, Kuriiwa T, Tamura T, Takamura H, Kamegawa K. Symmetry and hyperfine magnetic fields in Nd-based intermetallics. Intermetallics 2001;7:67.
[19] Yan Y, Chen Y, Liang H, Wu C, Tao M, Mingjing T. Effect of Al on hydrogen storage properties of $V_{30}Ti_{35}Cr_{25}Fe_{10}$ alloy. J Alloys Compds 2006;426:253–5.
[20] Cho SW, Park CN, Yoo JH, Choi J, Park JS, Suh CY. et al. Hydrogen absorption–desorption characteristics of $Ti_{(0.22+X)}Cr_{(0.28+1.5X)}V_{(0.5-2.5X)}$ ($0 \leqslant X \leqslant 0.12$) alloys. J Alloys Compds 2005;403:262–6.
[21] Kabutomori T, Takeda H, Wakisaka Y, Ohnishi K. Hydrogen absorption properties of Ti–Cr–A (A = V, Mo or other transition metal) BCC solid solution alloys. J Alloys Compds 1995;231:528–32.
[22] Klyamkin SN, Kovriga AY, Verbetsky VN. Effect of substitution on FCC and BCC hydride-phase formation in the $TiCr_2$–H_2 system. Int J Hydrogen Energy 1999;24:149–52.
[23] Uno M, Takahashi K, Maruyama T, Muta H, Yamanaka S. Hydrogen solubility of BCC titanium alloys. J Alloys Compds 2004;366:213–6.
[24] Huang T, Wu Z, Xia B, Huang T. Influence of V content on structure and hydrogen desorption performance of TiCrV-based hydrogen storage alloys. Mater Chem Phys 2005;93:544–7.
[25] Bloch J, Mintz MH. Kinetics and mechanisms of metal hydrides formation—a review. J Alloys Compds 1997;253–254:529–41.
[26] Hout J, Bouaricha S, Boily S, Dodelet JP, Guay D, Schulz RJ. Increase of specific surface area of metal hydrides by lixiviation. Alloys Compds 1998;266:307–10.
[27] Sandrock G. A panoramic overview of hydrogen storage alloys from a gas reaction point of view. J Alloys Compds 1999;293–295:877–88.